Ultramicroscopy 206 (2019) 112811

Contents lists available at ScienceDirect

Ultramicroscopy

journal homepage: www.elsevier.com/locate/ultramic

Localized surface curvature artifacts in tip-enhanced nanospectroscopy imaging

E. Sheremet[a], L. Kim[a], D. Stepanichsheva[a], V. Kolchuzhin[b,d], A. Milekhin[c], D.R.T. Zahn[d], R.D. Rodriguez[a,*]

[a] Tomsk Polytechnic University, 30 Lenin Ave, 634050 Tomsk, Russia
[b] Qorvo Munich GmbH, Konrad-Zuse-Platz 1, D-81829 Munich, Germany
[c] Rzhanov Institute of Semiconductor Physics of the Siberian Branch of the RAS, 630090 Novosibirsk, Russia
[d] Chemnitz University of Technology, D-09107 Chemnitz, Germany

ARTICLE INFO

Keywords:
TERS
Imaging artifacts
Plasmonics
Nanospectroscopy
Scanning probe microscopy

ABSTRACT

Tip-enhanced Raman spectroscopy (TERS) allows the chemical analysis with a spatial resolution at the nanoscale, well beyond what the diffraction limit of light makes possible. We can further boost the TERS sensitivity by using a metallic substrate in the so-called gap-mode TERS. In this context, the goal of this work is to provide a generalized view of imaging artifacts in TERS and near-field imaging that occur due to tip-sample coupling. Contrary to the case of gap-mode with a flat substrate where the size of the enhanced region is smaller than the tip size when visualizing 3D nanostructures the tip convolution effect may broaden the observed dimensions due to the local curvature of the sample. This effect is particularly critical considering that most works on gap-mode TERS consider a perfectly flat substrate which is rarely the case in actual experiments. We investigate a range of substrates to evidence these geometrical effects and to obtain an understanding of the nanoscale curvature role in TERS imaging. Our experimental results are complemented by numerical simulations and an analogy with atomic force microscopy artifacts is introduced. As a result, this work offers a useful analysis of gap-mode TERS imaging with tip- and substrate-related artifacts furthering our understanding and the reliability of near-field optical nanospectroscopy.

1. Introduction

The current progress in developing novel functional nanomaterials for upcoming technological applications depends critically on our ability to characterize these materials, their structure, and chemical composition with a spatial resolution better than 10 nm. In the same context, recent progress in coupling plasmonics with optical spectroscopy provided significant advancements in the characterization of chemical material composition with extraordinary sensitivity reaching a single-molecule level of detection [1–3]. Tip-enhanced Raman spectroscopy (TERS) is one of the most promising methods that combine single-molecule detection with spatially-resolved nanoscale mapping capabilities far beyond the diffraction limit of light [4–6].

In this context, the scanning tunneling microscope (STM) is the most convenient and robust technique that offers precise control over the plasmonically active gap formed between the metallic probe and a metalized substrate. Not surprisingly, several recent studies demonstrated remarkable achievements of STM-based TERS for chemical imaging with sub-nanometer resolution [5,7]. However, the STM-based TERS approach is limited to electrically conductive materials. Under ultra-high vacuum and cryogenic temperatures, STM-TERS allowed Zhang et al. to obtain submolecular resolution [8], while in ambient conditions image resolutions down to 1.7 nm [5] or in liquids can be achieved [9]. On the other hand, the atomic force microscopy (AFM)-based TERS approach is free of the limitations described above since the feedback-control is independent on the electrical conductivity of the sample. Therefore, AFM allows acquiring simultaneously three-dimensional maps of the sample morphology and two-dimensional hyperspectral Raman imaging, all these with nanoscale lateral resolution. The potential of AFM-TERS imaging in gap-mode was recently demonstrated by the Deckert's group, who identified the structure of a single peptide molecule and amyloid aggregates using this method [10,11].

It is now accepted that the *hotspots*, the regions providing Raman signal enhancement of the order of 10^7, usually appear in gaps formed between metallic nanostructures both in TERS [6] and in SERS configurations [6,12,13]. It was shown that even stronger enhancement up

* Corresponding author.
E-mail address: raul@tpu.ru (R.D. Rodriguez).

https://doi.org/10.1016/j.ultramic.2019.112811
Received 12 March 2019; Received in revised form 26 June 2019; Accepted 4 July 2019
Available online 04 July 2019
0304-3991/

to 10^{13} could be achieved using a combination of SERS and TERS in the so-called *gap-mode* TERS [7]. In this mode, the hotspot between a metalized scanning probe tip and a metallic substrate seems to be the key to reproducible nanoscale imaging.

However, the widespread and reliable implementation of TERS requires the understanding of imaging artifacts understood as misrepresentations of sample surface introduced by the instrument or technique used. Imaging artifacts can rise for multiple reasons such as light scattering by the tip [14,15], tip degradation or fluctuations of the enhancement factor over the surface [16]. The detected spectra can also differ significantly from the classical Raman spectra due to gap-mode plasmon luminescence [17], signal fluctuations of carbon contamination or single-molecules [16,18], suppression [19] or shift of particular Raman modes, and activation of forbidden ones [20].

Atomic force microscopy (AFM) introduces a new set of artifacts that, in turn, carry information about the tip itself when the structure size becomes comparable to the tip apex diameter [21]. Imaging artifacts and curvature effects are common-knowledge in the scanning probe microscopy community, but their role in TERS imaging and near-field optical enhancement was barely investigated. One should expect artifacts due to multiple particularities of the tip-sample interaction affecting the electric field enhancement. The large TERS signal enhancement in gap-mode TERS is due to the use of a metallic film rather than semiconducting or dielectric ones. This configuration was shown in a multitude of theoretical works and used in several experiments to improve the signal intensity and spatial resolution thanks to better spatial confinement of the electromagnetic field [22–25]. The effect is well explained by the image dipole model. The image dipole is affected by the changes in the substrate optical properties and is thoroughly described in the literature [22–25]. Thus, in the case of gold nanoclusters on a silicon substrate, we should expect higher enhancement over the gold-coated areas in the case of a perfectly flat surface. However, for sample surfaces that are not flat, we must consider the formation of the tip-substrate "hotspot" that will be determined by the tip and substrate local curvature, the resonance of the localized plasmon and its shift upon the tip-substrate coupling. Here, we provide an understanding of how these tip-substrate coupling artifacts affect the near-field optical properties reflected in TERS imaging. For this, we performed chemical mapping of metal phthalocyanine ultrathin layers (CoPc or CuPc) adsorbed on different metallic nanostructures. The nanoscale resolution hyperspectral imaging using gap-mode AFM-TERS allows studying the following cases:

1 Tip-sample coupling for isolated gold nanoclusters;
2 The change of surface curvature;
3 Tip over the surface with a negative curvature formed by metal films on nanospheres (MFON).

2. Experimental methods

2.1. Tip-enhanced Raman spectroscopy instrumentation

The TERS experiments were performed with atomic force microscopy in contact and intermittent-contact modes using gold metal probes (probes.ters-team.com) specially designed for AFM-based TERS [26]. The tip apex was etched electrochemically with the resulting tip radius of *ca.* 50 nm. Scanning electron microscopy (SEM) images of the TERS tips were obtained using NanoSEM 200 from FEI.

Two different setups were used, both in the side-illumination/collection configuration: A home-coupled TERS system with an Agilent 5420 AFM and a LabRam HR800 Raman spectrometer, and a dedicated TERS system OmegaScope-R from AIST-NT Inc. coupled to an Xplora Raman spectrometer. Raman spectroscopy was performed under red (633 nm and 638 nm) and green (514.7 nm) laser excitations. The measurements with red laser must be considered tip-enhanced resonant Raman spectroscopy (TERRS) since phthalocyanines exhibit an absorption peak at *ca.* 650 nm [27,28]. The light of 1 mW power was focused with a 50x LWD objective (N.A. 0.42) in the Agilent-HORIBA system, and 160 μW focused with a 100x LWD objective (N.A. 0.7) in the AIST-NT-Xplora HORIBA system. The power density was 105 and 133 W/mm^2 for the two experimental setups. A grating of 600 l/mm was used to disperse the scattered light on CCD detectors.

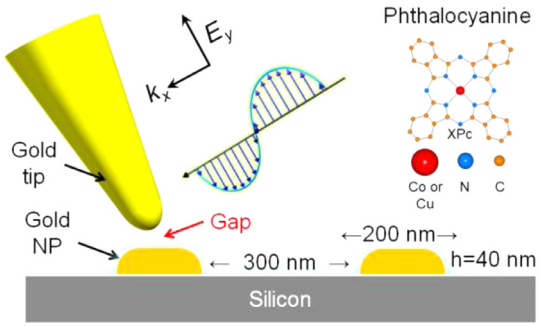

Fig. 1. Schematics of the TERS experiments on gold clusters formed using electron beam lithography. The substrate with a 500 nm period was covered by 2 nm of the metal phthalocyanine (XPc, X = Cu or Co).

2.2. Lithographically defined gold particles

SERS substrates with lithographically-defined clusters, sketched in Fig. 1, were fabricated by electron beam lithography; additional details can be found in previous works [29,30]. An electron resist (PMMA 950 K) deposited on a silicon (100) substrate was structured with an electron beam (Raith-150, Germany). The patterned resist was covered with 5 nm Ti and 40 nm Au films. Afterward, the remaining resist was removed by a lift-off process in dimethylformamide to obtain individual gold clusters on the surface. One section of this sample retained the Au layer on PMMA particles and on the Si substrate producing the sample shown in Fig. 2.

2.3. Metal film on nanosphere (MFON) substrate

The MFON substrate [31] was obtained by coating a silicon substrate by a monolayer of hexagonal closed-packed (hcp) polystyrene spheres with 450 nm diameter; additional details can be found in previous work [32]. The sample was partly metalized by evaporation of a 60 nm Au film. Half of the substrate was left without gold.

2.4. Organic layer deposition

The substrate was entirely covered by a 2 nm ("thin") of cobalt phthalocyanine (CoPc) or 40 nm ("thick") layer of copper phthalocyanine (CuPc) using organic molecular beam deposition (OMBD) under high vacuum ($\sim 10^{-7}$ mbar). The thickness of metal phthalocyanine films was controlled using a quartz crystal microbalance. The microbalance resonance shift *vs.* thickness was calibrated before the deposition by measuring the thickness of the reference layers by ellipsometry.

2.5. Numerical simulations

The commercial software ANSYS 14.0 Multiphysics was employed to analyze 3D models of the TERS tip and the substrate employing realistic configurations of the experiments. ANSYS Emag calculates the electromagnetic field components by finite element method (FEM) based on a full-wave formulation of Maxwell's equations in the harmonic regime.

The mesh was created with the HF119 tetrahedral element with a much finer mesh around the tip and the gap with the sample. Complex refractive index data for gold and silicon were used from a previous report [33]. The laser beam propagation was approximated by a plane

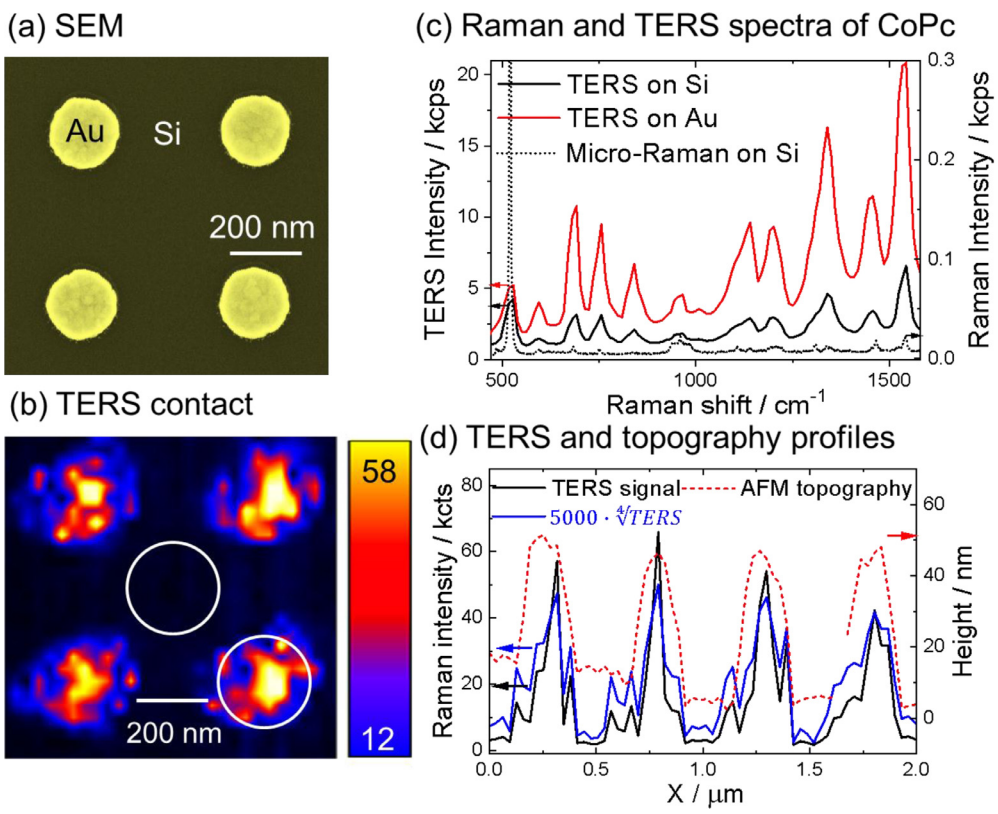

Fig. 2. Isolated disk-like gold nanocluster placed on a silicon substrate with parameters: height 40 nm, diameter 200 nm, analyzed with: (a) SEM; (b) TERS image obtained with 638 nm excitation wavelength following the intensity of the CoPc mode at 1540 cm^{-1}, the step size is 31 nm; (c) Averaged TERS spectra extracted from regions circled in (b) where the tip is on the gold particle (red) and spectra from the tip on the silicon substrate (black). The reference spectrum measured in micro-Raman configuration on a Si substrate is plotted by the dotted line; (d) Comparison of the AFM and TERS profiles over four Au nanoclusters. Along with TERS, the ¼ power of the signal is presented that is proportional to the electric field enhancement. The values are multiplied by 5000 to make a better profile comparison (similar scaling). (For interpretation of the references to color in this figure legend, the reader is referred to the web version of this article.)

electromagnetic wave with $\lambda = 633$ nm with an electric field amplitude of 1 V/m. The computational domain was truncated with a surface impedance absorbing boundary condition.

3. Results and discussion

3.1. The case of isolated Au particles

The SEM image of isolated gold nanoclusters on a silicon substrate is shown in Fig. 2a. The nanoclusters have a height of 40 nm, 200 nm diameter, and disk-like shape. The edges are rounded due to the limitations of electron beam lithography. The TERRS images for the most intense Raman feature of CoPc at 1540 cm^{-1} attributed to C=N stretching (Fig. 2c) taken from the same area for the case of isolated gold nanoclusters on a silicon substrate are shown in Fig. 2b. As expected from the extensive research on gap-mode TERS, the TERS signal from the 2 nm CoPc film is larger over the gold nanoclusters than on the Si substrate. The CoPc spectra remain unchanged as compared to the reference spectrum in Fig. 2c. The signal enhancement is inhomogeneous over the nanocluster surface due to its roughness. When comparing the spectra averaged over the circled areas in Fig. 2b, the signal intensity is at least 3 times higher over the gold nanoclusters and reaches up to 12 times enhancement at its maximum. TERS imaging shows, however, an interesting effect: the TERS enhancement is not equally distributed over the whole nanocluster surface and appears to be asymmetric. Such effects are not observed for the AFM profile obtained with the same tip (Fig. 2d) and are preserved when we consider the signal amplified as the 4th power of the electric field enhancement. Thus we can consider this effect as electromagnetic tip self-imaging analogous to the tip convolution effect known in the scanning probe microscopy (SPM) community [34,35]. We observe several changes in the TERS profile as compared to the AFM profile: (1) for all the nanoclusters the signal is much higher when the tip is above its center as compared to when the tip is above the edges; (2) the signal enhancement tends to extend beyond the nanocluster on the one side; (3) the enhancement appears to have very localized nature within the nanocluster area. The localized nature of the enhancement can be attributed to the grainy structure of the polycrystalline nanocluster surface that could also affect the CoPc distribution. These small topographic changes are obvious from the SEM image but are not visible in the AFM profile obtained with TERS tip suggesting that the TERS resolution outperforms AFM at least in gap-mode which was shown previously in multiple theoretical works. The two other artifacts must be considered on a larger scale and can be understood by performing numerical simulations of the tip at different positions over the Au nanocluster.

To consider the experimental asymmetry, the model geometry was approximated to the key experimental parameters. The tip apex radius, tip apex angle, and tip-tilt angle were determined from the SEM images of the tip used, and the cantilever tilt angle is known from the AFM instrument design. The experimental values for the incident angle of light and the illumination direction were also taken into account. The results are presented in Fig. 3. Intuitively, one expects the case 3 to provide the highest enhancement since the tip is aligned with the electric field of the p-polarized incident laser light, and the edge curvature should localize the electromagnetic field due to lightning rod effect. However, the simulations suggest that the field enhancement is the highest when the tip is above the center of the nanocluster, which also matches the experimental results. This effect results in a “tip narrowing artifact”. Note that in this case, the surface roughness of tip and nanoclusterdue to their polycrystallinity has been neglected still providing reasonably good matching between the theory and the experiment. However, since the plasmonic resonance frequency and electromagnetic field localization depend on the particular geometry of the tip, the interpretation of TERS images must always be supported by electromagnetic field simulations.

The asymmetry of the TERS profile is explained by the fact that one of the sides of the tilted tip interacts with the surface feature (the nanocluster in our case) leading to an apparent enlarged width of the measured structure on one side. The fact that this artifact is not

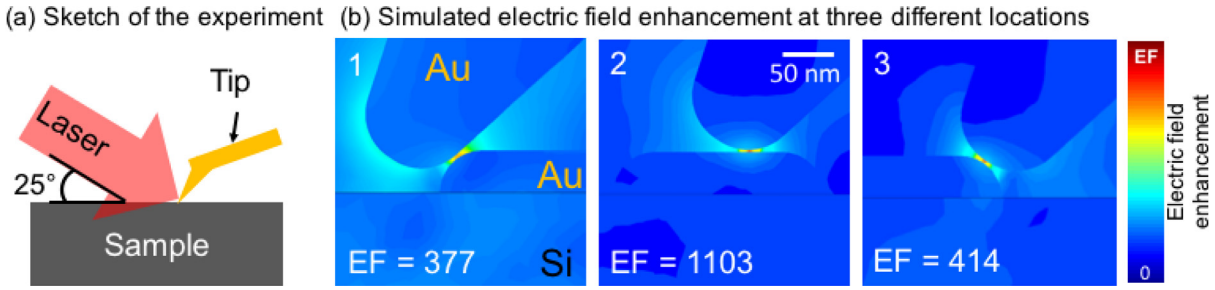

Fig. 3. FEM simulations to determine asymmetric effects of signal amplification of a gold nanocluster and a gold tip: (a) sketch of the geometry; (b) finite element method simulation for the tip in different locations with maximum enhancement factor EF for each configuration. The scale bar and the color scale are the same for all three simulated images, while the maximum EF is indicated in each of them.

observed in the AFM topography image suggests that the electromagnetic coupling extends beyond the AFM interaction analogously to the tip broadening artifact. This is in line with the known interaction distances of *ca.* 10 nm for electromagnetic field coupling and *ca.* 1–2 nm for the atomic forces [36].

3.2. The change of the surface curvature on a continuous film

In the previous case, we looked at isolated nanoclusters, which means that the effects may be partially determined by the localized surface plasmons. Further, we consider nanoclusters of the same size (200 nm diameter and 40 nm height) but located on a gold film instead of silicon. The sketch of the structure cross-section is presented in Fig. 4a. The surface curvature change was introduced by a polymer underneath the gold layer during the process of preparation by electron beam lithography. The resulting topography is seen in the AFM height image (Fig. 4b). Indeed, in the TERS experiment performed on this structure, the intensity of the CoPc B_{1g} mode at 682 cm^{-1} mapped in Fig. 2c increases by 25% when the Au TERS tip is moved to the Au film as compared to its intensity over the Si substrate. We also observed a 55% increase of the CoPc signal intensity over the surface features as compared to the Si substrate. Such cases are hard to analyze analytically, and there are only a few experimental reports in the literature [37]. Therefore, to complement our understanding of this configuration, we performed numerical simulations of a system mimicking the experimental conditions.

The FEM simulations of the Au tip were performed based on the tip radius of 30 nm experimentally determined from a scanning electron microscopy (SEM) analysis. The images in Fig. 5a–c are obtained for the systems made by an Au tip over a Si substrate, Au tip over a 40 nm thick Au film on Si, and a curved Au surface feature with parameters obtained from the AFM experiments (40 nm height and *ca.* 200 nm diameter in Fig. 4b). The distance between the tip and the sample of 2 nm corresponds to the nominal CoPc thickness. When comparing the local field enhancement for all three configurations, at the same excitation wavelength (633 nm), we observe a 3-fold and 6-fold enhancement of the electric field for the cases of the Au film and the curved surface with respect to the Au tip over the silicon substrate. The results are qualitatively explained by the image dipole model predicting higher field enhancement above a flat metallic surface and even higher over a protrusion [38]. We attribute the much lower contrast observed in the experiment (25 and 55%) as compared to the simulations (200 and 500%) to the fact that the TERS imaging experiment was performed with the tip oscillating in tapping mode. Thus, the enhancement was strong only during a small fraction of the oscillation cycle. Moreover, the high refractive index of CoPc film was omitted in the simulations. It naturally leads to damping of the electric field in the gap but would probably have no effect on the image contrast.

The gap formed by the tip and the metal substrate strongly confines the electric field under the tip in a nanometer range, increasing the sensitivity and spatial resolution in TERS experiments. This happens because the gap acting as a nano-antenna amplifies both the electric field of the excitation and the electric field of the Raman scattered light from the sample. The optical signal intensity that can be detected is

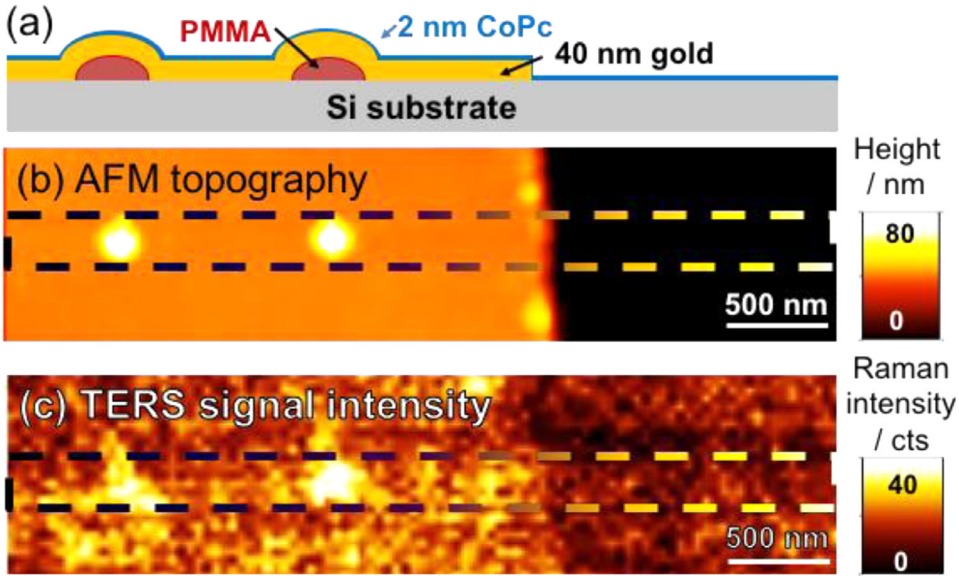

Fig. 4. TERS imaging of the sample with different surface curvature. (a) Sample cross-section; (b) AFM image of the surface; (c) TERS image of the mode at 682 cm^{-1}. The step size is 39 nm, excitation wavelength 632.8 nm.

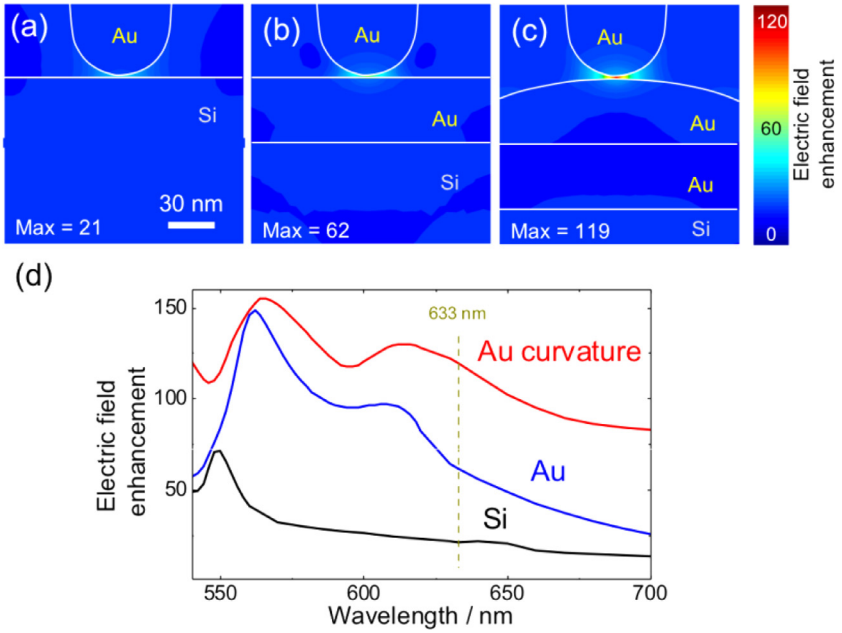

Fig. 5. Finite element method simulation of electric field amplification in the gap with a nanometer range acting as a nano-antenna between gold tip and different substrates: (a) flat silicon substrate; (b) silicon with a flat 40 nm gold film; (c) curved Au surface; (d) electric field amplitude magnification for a certain wavelength range.

proportional to the square of the electric field intensity. If both, the spectral regions of the scattered signal and the excitation are spectrally close to each other, then the difference in enhancement factors for both wavelengths can be neglected. In this case, the total increase in Raman intensity scales to the fourth power of the electric field enhancement. This condition is usually met in the experiments although deviations would occur for very sharp localized surface plasmon resonances (LSPR) and for Raman modes at large wavenumbers [32]. The simulation results show that the gap-mode can increase the magnitude of the enhancement from 1.9×10^5 (E_{max} = 21) to 1.5×10^7 (E_{max} = 62). This increase of two orders of magnitude is achieved simply by depositing a 40 nm gold film on the silicon substrate.

The high field enhancement over the *flat* gold surface can be understood by the well-established image dipole effect that also leads to the redshift of the LSPR mode due to the coupling with the image dipole from the substrate. Note that the enhancement is observed for all the wavelength range presented in Fig. 3d. Higher TERS enhancement above a *curved* surface can be explained by one of the two effects 1) LSPR coupling of the tip and the surface feature and 2) the lightning rod effect for the curved surface. Of course, these two effects are not mutually exclusive so that a combination of both is also possible. The lightning rod effect originates from a purely geometric factor that occurs in sharp tips of metal nanostructures [39]. Since the use of FEM implies the solution of Maxwell's equations numerically, the mathematical approach does not allow us to arbitrarily exclude one effect or the other. In general, since the boundary conditions require the electric field lines to be perpendicular to the surface of a perfect conductor, some field enhancement will occur on any curved surface, while its exact value will depend on the feature dimensions and its aspect ratio. The LSPR is distinguished by a pronounced electric field enhancement at its resonance frequency. When performing a wavelength sweep, we observe the enhancement over the whole spectral range, suggesting that the effect is more related to the lightning rod effect than to the LSPR coupling. Still, the redshift of the LSPR maxima is visible in Fig. 5d, and this is explained by the tip-sample field coupling. [40]

This result must be compared to the work of Chen et al. [37] where a small gold particle on a gold surface was imaged with TERS. There, the additional enhancement was attributed to the LSPR coupling, which seems to be a reasonable assumption for a small particle. Regardless of the mechanism, and this is the most crucial point of this work, when interpreting TERS imaging data, the presence of such curvature represents a clear case of an imaging artifact since without prior knowledge one cannot judge whether the higher signal is achieved due to a different amount of material, substrate properties, or the substrate shape. Therefore, one needs to take into account the topographic SPM data but also the thickness of the Raman scattering layer (CoPc in our case). With the increase in the thickness of the CoPc layer, we should expect a larger volume of CoPc material in the near-field of the tip, but also exponentially weaker coupling with the gold film. Consider the case when a molecule of interest is inhomogeneously covering a rough surface. In this case, the topographic data must be considered for the correct interpretation of the TERS images. This impact of substrate morphology in TERS imaging was first identified in 2007 by Zhang et al. [41]. although just now it is systematically studied.

3.3. TERS imaging on a substrate with negative curvature

We performed imaging of a 40 nm thick film of CuPc on MFON. The Raman spectrum in Fig. 6a is the average over a whole TERS map. Two spectral regions (blue and yellow in Fig. 6a) were used to construct the TERS images marked by arrows in Fig. 6b and d. The background image in Fig. 6b has little correlation with the topography so that we can exclude the tip scattering enhancement mechanism. The TERS intensity map of the C=C ring stretching mode around 1530 cm^{-1} in Fig. 6d shows the most significant signal enhancement over the highest regions of the AFM topography (Fig. 6c), but also a few regions with a low signal intensity that corresponds to a missing nanosphere and lower regions of the substrate. We find these large-scale signal changes hard to interpret reliably and attributethem to tip shadowing effects, film thickness, field enhancement variations, or slight optics instability over the large-scale image.

In contrast to the featureless map of the background intensity map shown in Fig. 6b, the TERS map in Fig. 6d displays regions with a subtle hexagonal arrangement. Notice also the difference in intensity scales between Fig. 6b and d. The hexagonal symmetry of the topography and TERS results are reflected in the fast Fourier transform of those images in Fig. 6e and f, respectively. The composite image in Fig. 6g was formed by overlapping the topography and TERS maps; the direction of the electromagnetic excitation and its polarization are shown by arrows. Fig. 6g suggests that due to the large film thickness reducing the tip-sample coupling, the contrast between the different points is much lower than for the previous cases discussed above. The profiles in

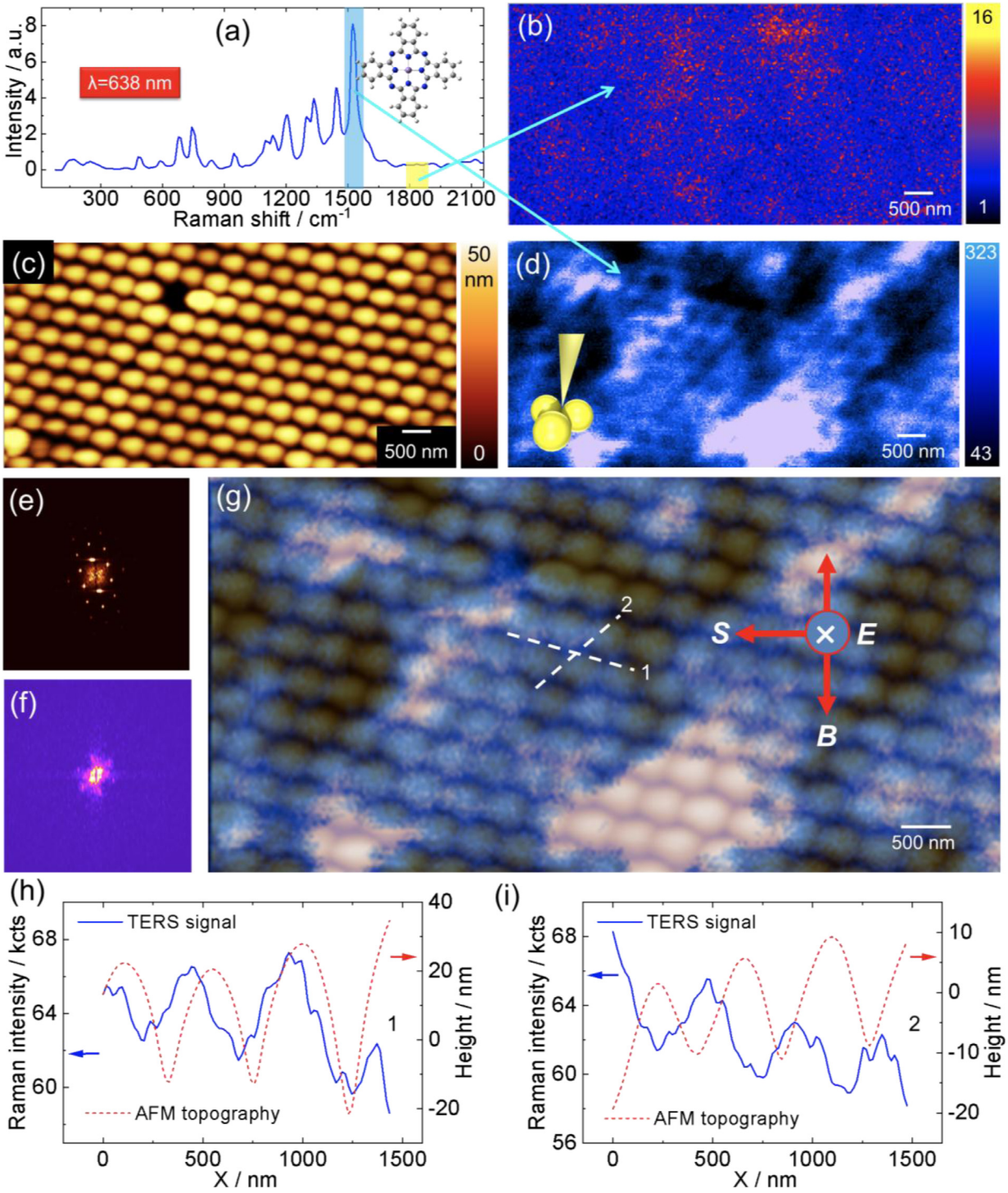

Fig. 6. (a) Raman spectra of a 40 nm CuPc film on the MFON substrate averaged over the entire spatial region mapped in TERS. The inset shows the scheme used for finite element method simulations of a gold tip over a gold particle under red excitation. The distance between the tip and particle is now set to 50 nm in the simulation showing that there is a persistent coupling between tip and sample. The flat region marked in the spectrum (yellow) was used to visualize the TERS map of the background in (b) with no contrast related to the surface topography shown in (c). While the intensity mapping of the main peak (blue) of the C=C vibration in (d) shows a faint but perceptible resemblance to the hexagonal close-packing of the MFON surface. The step size is 31 nm. (e) and (f) are the fast Fourier transforms of the topography (c) and TERS image (d), respectively. (g) is the composed image formed by overlapping the height and TERS images, the direction of laser excitation and its polarization are shown with red arrows. Profiles in (h) and (i) show the AFM topography and the TERS signal intensity along the dashed lines in (g). (For interpretation of the references to color in this figure legend, the reader is referred to the web version of this article.)

Fig. 6h and i show a spatial offset between the AFM topography and the TERS signal intensity. For the tip located between the spheres, two hot spots are expected to be generated, providing higher signal intensity in the offset position. The change of the illumination direction affects the different offsets in the two profiles.

3.4. Discussion and implications

The enhancement patterns in all three cases illustrate the difference in signal intensity that can be achieved when gap-mode is used on various substrates. This is a critical point for nanoscale spectroscopy imaging since larger signals imply that lower acquisition times can be used, thus enabling faster scanning. Pushing to detect every single scattered photon, or increasing the scattered signal intensity, *e.g.* by using gap-mode imaging, allows nanoscale mapping with a much better spatial resolution that is otherwise hampered by instrumental limitations such as thermal drift. However, this larger enhancement in gap-mode TERS comes at the price of artifacts such as tip-convolution and tip-self-imaging that originate from the electromagnetic coupling between the tip and the sample. We found that when these two are separated by a spacer such as a thick molecular layer, then the tip artifacts are also reduced in the near-field imaging.

Our TERS analysis complemented by numerical simulations allowed introducing an analogy with atomic force microscopy artifacts. As a result, our work offers a useful framework for the analysis of TERS images with substrate-related artifacts in TERS, and particularly in gap-mode, thus improving the understanding and reproducibility in the area of near-field optical nanospectroscopy. At the time of submission of this work, Wang and Kurouski reported similar findings to ours regarding the role of sample features in the emergence of tip-related artifacts in TERS imaging [42]. They used gold plates functionalized with p-nitrothiophenol and found that in the reduction of thiophenol, the Au plate edges have lower catalytic activity than the flat basal plane. Their conclusions resonate with our results emphasizing the role of topographical effects on TERS imaging. Nevertheless, our combined computational and experimental work involving different tip-sample configurations takes Wang and Kurouski's observations a step beyond by carefully showing how closely related these artifacts are to the near-field coupling between the tip and the sample in gap-mode TERS, and by additionally showing how these artifacts can be minimized by weakening the coupling.

Just like it happened for AFM, [33] we expect that the emergence of reference samples for the analysis of AFM-TERS artifacts would allow the system characterization and a more robust interpretation of near-field images. This is indeed our next goal in this exciting research field. By analogy with AFM where one can restore the tip shape from analyzing the imaged particle itself, one could expect the TERS image to provide information about the tip plasmonic properties. This was shown in TERS on carbon nanotubes (CNTs) that helped to deduce the orientation of the tip dipole [43].

4. Conclusions

In this work, we demonstrated that the optical field amplification that occurs due to a change in the radius of curvature of a substrate gives rise to near-field imaging artifacts. To aid in understanding the experimental results, we performed numerical modeling of various tip-sample configurations used in the experiments. The simulation results show that gap-mode allows for increasing the enhancement factor from 1.9×10^5 to 1.5×10^7. This additional gain is achieved by depositing 40 nm gold film on a silicon substrate. An even more significant gain is achieved with a change in the curvature of the surface that can be explained by several effects: LSPR-coupling, tip/surface characteristics, lightning rod effect for a curved surface, or a combination of all these. We encountered some limitations, especially that it is impossible to isolate any of these effects using numerical simulations. Experimentally, the nanoscale sample curvature implies the introduction of an imaging artifact; therefore, one cannot judge whether a high signal intensity is achieved due to a different amount of material, due to the chemical properties of the substrate, or because of the shape of the substrate.

In the case of isolated Au nanoclusters, the signal on the CoPc film is 12 times larger than on the Si substrate, but the spatial distribution of the electric field enhancement is unevenly extending beyond the nanocluster surface. This effect is called tip convolution and arises from the interaction of the side walls of the tip with the surface feature (the nanocluster). The results show that a weak coupling in the gap-mode is still present through a thick organic layer >40 nm and that this reduction in the electromagnetic coupling also reduces the tip-convolution artifacts. We further discussed the implications of our work in the selective catalytic interaction of oxygen with CoPc at the nanoparticles edges as defined by the tip-sample geometry. Thus, this result is relevant to other areas in which TERS is starting making an impact like in heterogeneous catalysis. Our work shows that the significant increase of Raman intensity when using gap-mode TERS comes at the cost of imaging artifacts in the near-field. These artifacts also appear when imaging three-dimensional nano-objects becoming a contributor to the image contrast in TERS that should not be neglected.

Acknowledgments

We thank Ekaterina Rodyakina for providing the Au nanocluster array samples, Stefan Moras for the MFON samples, and Andrey Krayev for assistance and critical support with the TERS results. This work was supported by the DFG Research Unit FOR1713 SMINT, the Cluster of Excellence “Center for Advancing Electronics Dresden” (cfaed), and the RFBR projects 18-42-700014, 19-52-12041, and 18-02-00615. This work is funded by the Tomsk Polytechnic University Competitiveness Enhancement Program grant and supported by the Ministry of Education and Science of the Russian Federation.

Supplementary materials

Supplementary material associated with this article can be found, in the online version, at doi:10.1016/j.ultramic.2019.112811.

References

[1] B. Schreiber, D. Gkogkou, L. Dedelaite, J. Kerbusch, R. Hübner, E. Sheremet, et al., Large-scale self-organized gold nanostructures with bidirectional plasmon resonances for SERS, RSC Adv. 8 (2018) 22569–22576.
[2] S.-C. Luo, K. Sivashanmugan, J.-D. Liao, C.-K. Yao, H.-C. Peng, Nanofabricated SERS-active substrates for single-molecule to virus detection in vitro: a review, Biosens. Bioelectron. 61 (2014) 232–240.
[3] H. Cang, A. Labno, C. Lu, X. Yin, M. Liu, C. Gladden, et al., Probing the electromagnetic field of a 15-nanometre hotspot by single molecule imaging, Nature 469 (2011) 385–388.
[4] B. Pettinger, Single-molecule surface- and tip-enhanced raman spectroscopy, Mol. Phys. 108 (2010) 2039–2059.
[5] C. Chen, N. Hayazawa, S. Kawata, A 1.7 nm resolution chemical analysis of carbon nanotubes by tip-enhanced Raman imaging in the ambient, Nat. Commun. 5 (2014) 3312.
[6] B. Pettinger, P. Schambach, C.J. Villagómez, N. Scott, Tip-enhanced raman spectroscopy: near-fields acting on a few molecules, Annu. Rev. Phys. Chem. 63 (2012) 379–399.
[7] J.M. Marr, Z.D. Schultz, Imaging electric fields in SERS and TERS using the vibrational stark effect, J. Phys. Chem. Lett. 4 (2013), https://doi.org/10.1021/jz401551u.
[8] R. Zhang, Y. Zhang, Z.C. Dong, S. Jiang, C. Zhang, L.G. Chen, et al., Chemical mapping of a single molecule by plasmon-enhanced Raman scattering, Nature 498 (2013) 82–86.
[9] T. Touzalin, A.L. Dauphin, S. Joiret, I.T. Lucas, E. Maisonhaute, Tip enhanced Raman spectroscopy imaging of opaque samples in organic liquid, Phys. Chem. Chem. Phys. 18 (2016) 15510–15513.
[10] T. Deckert-Gaudig, E. Bailo, V. Deckert, Tip-enhanced Raman scattering (TERS) of oxidised glutathione on an ultraflat gold nanoplate, Phys. Chem. Chem. Phys. 11 (2009) 7360–7362.
[11] A.V. Krasnoslobodtsev, T. Deckert-Gaudig, Y. Zhang, V. Deckert, Y.L. Lyubchenko, Polymorphism of amyloid fibrils formed by a peptide from the yeast prion protein Sup35: AFM and tip-enhanced Raman scattering studies, Ultramicroscopy 165 (2016) 26–33.
[12] S. Schluecker, ChemInform abstract: surface-enhanced Raman spectroscopy: concepts and chemical applications, ChemInform. 45 (2014) no–no.
[13] S.L. Kleinman, R.R. Frontiera, A.-I. Henry, J.A. Dieringer, R.P. Van Duyne, Creating, characterizing, and controlling chemistry with SERS hot spots, Phys. Chem. Chem. Phys. 15 (2013) 21–36.
[14] R. Ramos, M.J. Gordon, Near-field artifacts in tip-enhanced Raman spectroscopy,

Appl. Phys. Lett. 100 (2012) 213111.
[15] N. Kumar, A. Rae, D. Roy, Accurate measurement of enhancement factor in tip-enhanced Raman spectroscopy through elimination of far-field artefacts, Appl. Phys. Lett. 104 (2014) 123106.
[16] E. Bortchagovsky, T. Schmid, R. Zenobi, Internal standard for tip-enhanced Raman spectroscopy, Appl. Phys. Lett. 103 (2013) 043111.
[17] B. Pettinger, K.F. Domke, D. Zhang, R. Schuster, G. Ertl, Direct monitoring of plasmon resonances in a tip-surface gap of varying width, Phys. Rev. B Condens. Matter. Am. Phys. Soc. 76 (2007) 113409.
[18] K.F. Domke, D. Zhang, B. Pettinger, Enhanced Raman spectroscopy: single molecules or carbon? J. Phys. Chem. C 111 (2007) 8611–8616.
[19] D. Kurouski, T. Postiglione, T. Deckert-Gaudig, V. Deckert, I.K. Lednev, Amide I vibrational mode suppression in surface (SERS) and tip (TERS) enhanced Raman spectra of protein specimens, Analyst 138 (2013) 1665–1673.
[20] M. Sun, Y. Fang, Z. Zhang, H. Xu, Activated vibrational modes and Fermi resonance in tip-enhanced Raman spectroscopy, Phys. Rev. E Stat. Nonlin. Soft Matter Phys. 87 (2013) 020401.
[21] C. Wong, P.E. West, K.S. Olson, M.L. Mecartney, N. Starostina, Tip dilation and AFM capabilities in the characterization of nanoparticles, JOM 59 (2007) 12–16.
[22] J. Stadler, B. Oswald, T. Schmid, R. Zenobi, Characterizing unusual metal substrates for gap-mode tip-enhanced Raman spectroscopy, J. Raman Spectrosc. 44 (2012) 227–233.
[23] N. Behr, M.B. Raschke, Optical antenna properties of scanning probe tips: plasmonic light scattering, tip−sample coupling, and near-field enhancement, J. Phys. Chem. C 112 (2008) 3766–3773.
[24] R.T. Hill, J.J. Mock, Y. Urzhumov, D.S. Sebba, S.J. Oldenburg, S.-Y. Chen, et al., Leveraging nanoscale plasmonic modes to achieve reproducible enhancement of light, Nano Lett. 10 (2010) 4150–4154.
[25] Principles of nano-optics, Nano Today 1 (2006) 41.
[26] R.D. Rodriguez, E. Sheremet, S. Müller, O.D. Gordan, A. Villabona, S. Schulze, et al., Compact metal probes: a solution for atomic force microscopy based tip-enhanced Raman spectroscopy, Rev. Sci. Instrum. 83 (2012) 123708.
[27] C.G. Claessens, U. Hahn, T. Torres, Phthalocyanines: from outstanding electronic properties to emerging applications, The Chem. Record 8 (2008) 75–97.
[28] A.T. Davidson, The effect of the metal atom on the absorption spectra of phthalocyanine films, J. Chem. Phys. 77 (1982) 168–172.
[29] E. Sheremet, A.G. Milekhin, R.D. Rodriguez, T. Weiss, M. Nesterov, E.E. Rodyakina, et al., Surface- and tip-enhanced resonant Raman scattering from CdSe nanocrystals, Phys. Chem. Chem. Phys. 17 (2015) 21198–21203.
[30] E. Sheremet, R.D. Rodriguez, D.R.T. Zahn, A.G. Milekhin, E.E. Rodyakina, A.V. Latyshev, Surface-enhanced Raman scattering and gap-mode tip-enhanced Raman scattering investigations of phthalocyanine molecules on gold nanostructured substrates, J. Vac. Sci. Technol. B Nanotechnol. Microelectr. 32 (2014) 04E110.
[31] L.A. Dick, A.D. McFarland, C.L. Haynes, R.P. Van Duyne, Metal film over nanosphere (MFON) electrodes for surface-enhanced Raman spectroscopy (SERS): improvements in surface nanostructure stability and suppression of irreversible loss, J. Phys. Chem. B 106 (2002) 853–860.
[32] R.D. Rodriguez, E. Sheremet, M. Nesterov, S. Moras, M. Rahaman, T. Weiss, et al., Aluminum and copper nanostructures for surface-enhanced Raman spectroscopy: a one-to-one comparison to silver and gold, Sens. Actuators B Chem. 262 (2018) 922–927.
[33] H. Itoh, T. Fujimoto, S. Ichimura, Tip characterizer for atomic force microscopy, Rev. Sci. Instrum. 77 (2006) 103704.
[34] R.D. Rodriguez, E. Lacaze, J. Jupille, Probing the probe: AFM tip-profiling via nanotemplates to determine Hamaker constants from phase–distance curves, Ultramicroscopy 121 (2012) 25–30.
[35] P.-E. Mazeran, L. Odoni, J.-L. Loubet, Curvature radius analysis for scanning probe microscopy, Surf. Sci. 585 (2005) 25–37.
[36] Y. Seo, W. Jhe, Atomic force microscopy and spectroscopy, Rep. Prog. Phys. 71 (2008) 016101.
[37] J. Chen, W. Yang, K. Dick, K. Deppert, H.Q. Xu, L. Samuelson, et al., Tip-enhanced Raman scattering of p-thiocresol molecules on individual gold nanoparticles, Appl. Phys. Lett. 92 (2008) 093110.
[38] E.G. Bortchagovsky, Simple modeling of the ratio of fields at a tip and at contacting surface [Internet], Nanospectroscopy (2016), https://doi.org/10.1515/nansp-2016-0002.
[39] P.F. Liao, A. Wokaun, Lightning rod effect in surface enhanced Raman scattering, J. Chem. Phys. 76 (1982) 751–752.
[40] Surface enhanced raman spectroscopy: analytical, biophysical and life science applications [Internet], in: J. Homola, Sebastian Schlücker (Eds.), Surface enhanced raman spectroscopy: analytical, biophysical and life science applications [Internet], Anal. Bioanal. Chem. (2011) 2329–2330, https://doi.org/10.1007/s00216-011-5321-8.
[41] W. Zhang, X. Cui, B.-S. Yeo, T. Schmid, C. Hafner, R. Zenobi, Nanoscale roughness on metal surfaces can increase tip-enhanced Raman scattering by an order of magnitude, Nano Lett. 7 (2007) 1401–1405.
[42] R. Wang, D. Kurouski, Elucidation of tip-broadening effect in tip-enhanced raman spectroscopy (TERS): a cause of artifacts or potential for 3D TERS, J. Phys. Chem. C (2018), https://doi.org/10.1021/acs.jpcc.8b09455.
[43] T. Mino, Y. Saito, P. Verma, Quantitative analysis of polarization-controlled tip-enhanced Raman imaging through the evaluation of the tip dipole, ACS Nano. 8 (2014) 10187–10195.